Static behavior of thermally loaded multilayered Magneto-Electro-Elastic beam

M. Vinyas and S.C. Kattimani[*]

Department of Mechanical Engineering, National Institute of Technology Karnataka, Surathkal, 575025, India

Abstract. The present article examines the static response of multilayered magneto-electro-elastic (MEE) beam in thermal environment through finite element (FE) methods. On the basis of the minimum total potential energy principle and the coupled constitutive equations of MEE material, the FE equilibrium equations of cantilever MEE beam is derived. Maxwell's equations are considered to establish the relation between electric field and electric potential; magnetic field and magnetic potential. A simple condensation approach is employed to solve the global FE equilibrium equations. Further, numerical evaluations are made to examine the influence of different in-plane and through-thickness temperature distributions on the multiphysics response of MEE beam. A parametric study is performed to evaluate the effect of stacking sequence and different temperature profiles on the direct and derived quantities of MEE beam. It is believed that the results presented in this article serve as a benchmark for accurate design and analysis of the MEE smart structures in thermal applications.

Keywords: coupled properties; finite element; magneto-electro-elastic; potential, thermal loads

1. Introduction

Extensive interest has been stimulated among the researchers since Van Run *et al.* (1974) demonstrated the effective coupling properties of magneto-electro-elastic (MEE) materials for the first time. These typical materials develop the electric polarization and magnetization with the application of external magnetic field and electric field, respectively. Further, a significant interaction of the mechanical field with the electric and magnetic fields can also be noticed. More interestingly, they exhibit magneto-electric effect which is generally absent in the monolithic piezoelectric and piezomagnetic materials. Thus, the obtained magneto-electric effect through the elastic field results into the complete magneto-electro-elastic coupling. It promotes energy conversion between mechanical, electrical, magnetic and thermal fields which makes it adaptable for potential engineering applications such as sensors, actuators, energy harvesters, structural health monitors, non-volatile memories, photovoltaic etc. More frequently, precise performance of MEE structures is expected in harsh environmental conditions like thermal environment. Meanwhile, in the thermal environment, the MEE materials exhibit pyroeffects which refers to the added coupling between thermo-magnetic fields and thermo-electric fields. The presence of temperature leads to a vigorous change in the behaviour of MEE structures in terms of stresses, displacements, and potentials. Hence, it is crucial to evaluate the multiphysics behaviour of MEE structures in various thermal environments.

The drastic developments in the material science technology and increased utilization of MEE materials in smart structures have paved way for numerous research works on investigating the coupled response of MEE structures. In this regard, various computational methods are being exploited to determine the free vibration and static behaviour of MEE structures. It includes analytical approach, state space approach, discrete singular convolution (DSC), differential quadrature (DQ) methods etc. Pan and Heyliger (2002, 2003) derived an exact solution in the 3D domain to tackle the problem of free vibration and bending characteristics of MEE laminates. Using layerwise modeling approach, finite element (FE) solutions were presented (Lage *et al.* 2004, Phoenix *et al.* 2009) with respect to 2-D plate theories. Although, layerwise modeling yields higher accuracy, as the number of layer increases it leads to increased computational costs. For the magneto-electric coupled state, it is predicted that the elastic waves transverse comparatively slower than magneto-electric waves. Hence, the quasi-static approximation of the corresponding fields has to be considered. With the assumption of quasi-static state, Kuang (2011) studied the coupled behaviour of thin MEE plate, using first order shear deformation theory (FSDT).

Meanwhile, to overcome the hurdles of layerwise modeling, equivalent single layer theories were proposed in conjunction with quasi-static approximations (Moita *et al.* 2009, Milazzo *et al.* 2009, Milazzo 2012, Milazzo and Orlando 2012). In addition, Alaimo *et al.* (2014) formulated multilayered MEE plate model to examine the large deflections in the MEE plate. In this regard, they used FE method together with FSDT. Sladek (2013), Xue *et al.* (2011) analysed the large deflections of homogeneous MEE plate using Petrov-Galerkin method and Bubnov-Galerkin method, respectively. Huang *et al.* (2010) investigated the static behaviour of functionally graded (FG) MEE beam subjected to sinusoidal loading. Buchanan (2004) has

---

*Corresponding author, Ph.D. Student
E-mail: sck@nitk.ac.in

studied the behaviour of layered versus multiphase magneto-electro-elastic infinite long plate composites by FE method. By using potential functions, Wang and Shen (2002) presented a general solution for 3D problems related to MEE media. Ramirez *et al.* (2006) examined the free vibration problem of the 2D MEE plates. Hosseini and Dini (2015) presented an analytical solution to investigate the magneto-thermo-elastic response of FG cylinder. Mahieddine and Quali (2008) presented a FE formulation of a beam with the piezoelectric patch. Razavi and Shooshtari (2015) considered von-Karman nonlinear strains and FSDT to study the nonlinear free vibration of MEE plates. Daga *et al.* (2009) investigated the transient dynamic response of MEE beam. Kattimani and Ray (2014a, b) analysed the active control geometrically nonlinear vibrations of MEE plates and doubly curved shells. They also extended their study for the FG MEE plates (2015). Free vibration characteristics of FG MEE plates were studied by Bhangale *et al.* (2006) with the aid of semi analytical FE procedure. Few researchers exploited the state space approach in order to evaluate the coupled response of MEE structures (Chen *et al.* 2005, Wang *et al.* 2003, Chen *et al.* 2007). Further, Xin and Hu (2015) evaluated the natural frequencies of the layered MEE beams by semi analytical state space approach.

In recent years, the research community is motivated to explore the behaviour of nanostructures. Using non-local theory in conjunction with Timoshenko beam theory, the frequency characteristics of MEE nanobeam was investigated by Ke and Wang (2014). Similarly, Ke *et al.* (2014) investigated the free vibrations of MEE nano plate with the help of Kirchhoff plate theory. Li *et al.* (2014) examined the effect of the elastic foundation on buckling and free vibration of MEE nanoplate through nonlocal Mindlin theory. Meanwhile, considering the influence of thermal environment, Ebrahimi and Barati (2016a, b) analysed the free vibration behaviour magneto-electro-thermo-elastic (METE) nanobeams. Ebrahimi and Jafari (2016) evaluated the thermo-mechanical vibrations of porous FG beam in the thermal environment. The forced vibration behaviour of METE nanobeams was studied by Ansari *et al.* (2015) by using von Karman nonlinearity. Barati and Shahverdi (2016) explored the effect of linear and non-linear temperature distribution on the thermal vibration of FG nonlocal plates. Further, many works have been reported on analyzing the nano and micro structures using DSC and DQ techniques. Based on strain gradient theory Akgöz and Civalek (2013, 2015) developed a new size dependant beam model and evaluated the bending and buckling behaviour of micro beams embedded in the elastic medium. They extended their investigation to study the buckling behaviour of linearly tapered micro columns using Bernoulli- Euler beam theory. Civalek *et al.* (2009) investigated the buckling analysis of Kirchhoff plate using DSC technique. Akgöz and Civalek (2015) used DSC approach and evaluated the bending response of FG microbeams, in conjunction with different beam theories. Civalek *et al.* (2009) studied the static analysis of carbon nanotubes in association with the Bernoulli-Euler beam theory. Kaghazian *et al.* (2017) solved the natural frequency problem of piezoelectric nanobeam using DQ technique.

Abundant research has been devoted in analyzing the behaviour of MEE structures exposed to the thermal environment. Among them, Sunar *et al.* (2002) proposed a finite element formulation for fully coupled thermopiezomagnetic continuum. Kumaravel *et al.* (2007) figured out the effect of temperature loads on the free vibration and linear buckling of the MEE beam. Taking into consideration, the influence of pyroeffects, Kondaiah *et al.* (2012, 2013) investigated the static behavior of MEE beams and plates subjected to a uniform temperature. Using FSDT Badri and Kayiem (2013) evaluated the coupled response of magneto-thermo-electro-elastic (MTEE) plates.

From the comprehensive literature survey, it is revealed that only a few articles have been reported on the static analysis of MEE beam in the thermal environment. To be specific, no attempt has been made on analyzing the influence of different temperature profiles on the static parameters of a multilayered MEE beam using FE method. In addition, it is noteworthy to mention that in contrast with other computational techniques, the 3D FE method can model the coupled physical system more accurately. The application of 3D elements would enable the representation of governing equations in all three axes, achieving accurate results. Also, geometric, constitutive and loading assumptions required for dimensionality reduction are avoided. Since the loading conditions in the real working environment are very likely to be 3D, the boundary conditions on both forces and displacements can be realistically treated. Therefore, 3D FE models represent more realistic geometric refinements and they are considered to be more reliable. Hence, through this article,
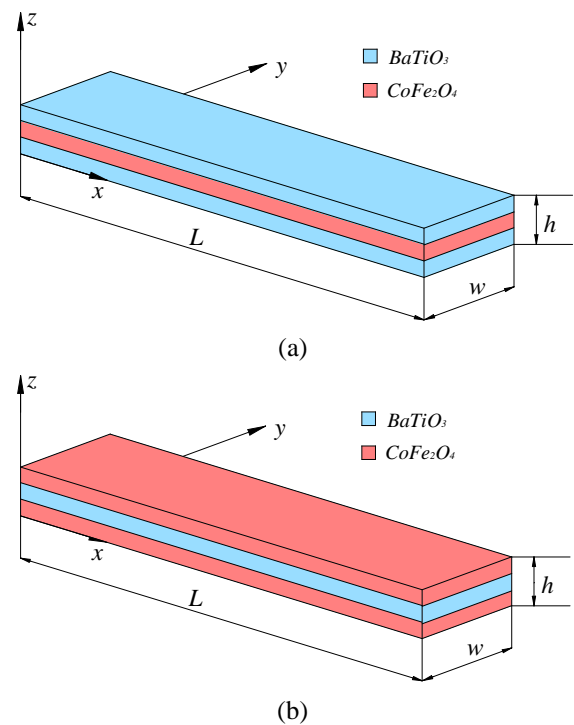

(a)

(b)

Fig. 1 Multilayered (a) BFB-MEE beam (b) FBF-MEE beam

an attempt has been made to develop a 3D FE formulation to study the static behaviour of the multilayered MEE beam in the different thermal environment. A parametric study is also carried out to evaluate the influence of the stacking sequence, temperature profiles on the displacements, potentials and the stresses.

2. Problem description

Assume a magneto-electro-elastic (MEE) beam made of Barium Titanate (BaTiO$_3$) and Cobalt Ferric oxide (CoFe$_2$O$_4$). The x, y and z axes of the Cartesian coordinate adjoin the length L, width w and thickness h, respectively, as depicted in Fig. 1. In the present analysis, two conventional stacking sequences are considered. They are *BFB* MEE beam and *FBF* MEE beam, where *B* denotes purely piezoelectric phase and *F* denotes purely piezomagnetic phase. In *BFB* MEE beam, the top and bottom layers are made of purely piezoelectric phase (BaTiO$_3$) and middle layer is composed of purely piezomagnetic phase (CoFe$_2$O$_4$), as shown in Fig. 1(a). Analogously, in *FBF* MEE beam, the top and bottom layers are purely piezomagnetic phase, whereas the middle layer is purely piezoelectric phase as illustrated in Fig. 1(b). The boundary conditions employed for the cantilever MEE beam is given by

$$u = v = w = \phi = \psi = 0 \quad \text{at} \quad x = 0$$
$$u = v = w = \phi = \psi \neq 0 \quad \text{at} \quad x = L \quad (1)$$

2.1 Constitutive equations

The linearly coupled constitutive relation of the MEE solid can be represented as follows

$$\{\sigma^k\} = \left[C_{V_f}^k\right]\{\varepsilon^k\} - \left[e_{V_f}^k\right]\{E^k\} - \left[q_{V_f}^k\right]\{H^k\} - \left[C_{V_f}^k\right]\{\alpha_{V_f}^k\}\Delta T$$

$$\{D^k\} = \left[e_{V_f}^k\right]^T\{\varepsilon^k\} + \left[\eta_{V_f}^k\right]\{E^k\} + \left[m_{V_f}^k\right]\{H^k\} + \{p_{V_f}^k\}\Delta T$$

$$\{B^k\} = \left[q_{V_f}^k\right]^T\{\varepsilon^k\} + \left[m_{V_f}^k\right]\{E^k\} + \left[\mu_{V_f}^k\right]\{H^k\} + \{\tau_{V_f}^k\}\Delta T$$

$$(2)$$

where, $\{\sigma^k\}$, $\{D^k\}$ and $\{B^k\}$, denotes the stress tensor, electric displacement and the magnetic flux, respectively; $\left[C_{V_f}^k\right]$, $\left[e_{V_f}^k\right]$, $\left[q_{V_f}^k\right]$, and $\{\alpha_{V_f}^k\}$ are the elastic co-efficient matrix, piezoelectric coefficient matrix, magnetostrictive coefficient matrix and thermal expansion co-efficient matrix, respectively; $\left[\eta_{V_f}^k\right]$, $\left[m_{V_f}^k\right]$, $\{p_{V_f}^k\}$, $\{\tau_{V_f}^k\}$ and $\left[\mu_{V_f}^k\right]$ are the dielectric constant, electromagnetic coefficient, pyroelectric constant, pyromagnetic constant and magnetic permeability constant, respectively; $\{\varepsilon^k\}$, $\{E^k\}$ and $\{H^k\}$ are the linear strain tensor, electric field and magnetic field, respectively. The temperature change is denoted by ΔT. In the above terms k represents the layer number and the subscript V_f denotes the volume fraction of BaTiO$_3$ and CoFe$_2$O$_4$ corresponding to the kth layer.

The non-zero components of various tensors appearing in Eq. (2) can be shown as follows

$$\begin{Bmatrix} \sigma_1 \\ \sigma_2 \\ \sigma_3 \\ \tau_{23} \\ \tau_{13} \\ \tau_{12} \end{Bmatrix} = \begin{bmatrix} c_{11} & c_{12} & c_{13} & 0 & 0 & 0 \\ c_{12} & c_{11} & c_{13} & 0 & 0 & 0 \\ c_{13} & c_{13} & c_{33} & 0 & 0 & 0 \\ 0 & 0 & 0 & c_{44} & 0 & 0 \\ 0 & 0 & 0 & 0 & c_{44} & 0 \\ 0 & 0 & 0 & 0 & 0 & c_{66} \end{bmatrix} \begin{Bmatrix} \varepsilon_1 \\ \varepsilon_2 \\ \varepsilon_3 \\ \gamma_{23} \\ \gamma_{13} \\ \gamma_{12} \end{Bmatrix} - \begin{Bmatrix} \alpha_1\Delta T \\ \alpha_2\Delta T \\ \alpha_3\Delta T \\ 0 \\ 0 \\ 0 \end{Bmatrix}$$

$$- \begin{bmatrix} 0 & 0 & e_{31} \\ 0 & 0 & e_{31} \\ 0 & 0 & e_{33} \\ 0 & e_{15} & 0 \\ e_{15} & 0 & 0 \\ 0 & 0 & 0 \end{bmatrix} \begin{Bmatrix} E_1 \\ E_2 \\ E_3 \end{Bmatrix} - \begin{bmatrix} 0 & 0 & q_{31} \\ 0 & 0 & q_{31} \\ 0 & 0 & q_{33} \\ 0 & q_{15} & 0 \\ q_{15} & 0 & 0 \\ 0 & 0 & 0 \end{bmatrix} \begin{Bmatrix} H_1 \\ H_2 \\ H_3 \end{Bmatrix} \quad (3.a)$$

$$\begin{Bmatrix} D_1 \\ D_2 \\ D_3 \end{Bmatrix} = \begin{bmatrix} 0 & 0 & e_{31} \\ 0 & 0 & e_{31} \\ 0 & 0 & e_{33} \\ 0 & e_{15} & 0 \\ e_{15} & 0 & 0 \\ 0 & 0 & 0 \end{bmatrix}^T \begin{Bmatrix} \varepsilon_1 \\ \varepsilon_2 \\ \varepsilon_3 \\ \gamma_{23} \\ \gamma_{13} \\ \gamma_{12} \end{Bmatrix} + \begin{bmatrix} \eta_{11} & 0 & 0 \\ 0 & \eta_{11} & 0 \\ 0 & 0 & \eta_{33} \end{bmatrix}$$

$$\begin{Bmatrix} E_1 \\ E_2 \\ E_3 \end{Bmatrix} + \begin{bmatrix} m_{11} & 0 & 0 \\ 0 & m_{11} & 0 \\ 0 & 0 & m_{33} \end{bmatrix} \begin{Bmatrix} H_1 \\ H_2 \\ H_3 \end{Bmatrix} + \begin{Bmatrix} p_1 \\ p_2 \\ p_3 \end{Bmatrix}\Delta T \quad (3b)$$

$$\begin{Bmatrix} B_1 \\ B_2 \\ B_3 \end{Bmatrix} = \begin{bmatrix} 0 & 0 & q_{31} \\ 0 & 0 & q_{31} \\ 0 & 0 & q_{33} \\ 0 & q_{15} & 0 \\ q_{15} & 0 & 0 \\ 0 & 0 & 0 \end{bmatrix}^T \begin{Bmatrix} \varepsilon_1 \\ \varepsilon_2 \\ \varepsilon_3 \\ \gamma_{23} \\ \gamma_{13} \\ \gamma_{12} \end{Bmatrix} + \begin{bmatrix} m_{11} & 0 & 0 \\ 0 & m_{11} & 0 \\ 0 & 0 & m_{33} \end{bmatrix}$$

$$\begin{Bmatrix} E_1 \\ E_2 \\ E_3 \end{Bmatrix} + \begin{bmatrix} \mu_{11} & 0 & 0 \\ 0 & \mu_{11} & 0 \\ 0 & 0 & \mu_{33} \end{bmatrix} \begin{Bmatrix} H_1 \\ H_2 \\ H_3 \end{Bmatrix} + \begin{Bmatrix} \tau_1 \\ \tau_2 \\ \tau_3 \end{Bmatrix}\Delta T \quad (3c)$$

2.2 Finite element formulation

A relationship can be established between generalized vectors ($\{d_t\}$, $\{\phi\}$ and $\{\psi\}$) and nodal vectors with the aid of shape function matrices as follows

$$\{d_t\} = \left[N_t\right]\{d_t^e\},$$
$$\{\phi\} = \left[N_\phi\right]\{\phi^e\}, \quad (4)$$
$$\{\psi\} = \left[N_\psi\right]\{\psi^e\}$$

where, the different shape function matrices are represented by

$$[N_t] = [N_{t1} \ N_{t2} \ \dots \ N_{t8}], \ N_{ti} = n_i I_t \ ,$$

$$[N_\phi] = [n_1 \ n_2 \dots n_8], \ [N_\psi] = [n_1 \ n_2 \dots n_8] \quad (5)$$

in which, n_i is the natural coordinate shape function associated with the ith node of the element; 'I_t' is the identity matrix; $[N_t]$, $[N_\phi]$ and $[N_\psi]$ are the shape function matrices, respectively. The linear relation between the electric field and the electric potential can be expressed as

$$E = -\nabla\phi \quad (6a)$$

Similarly, the magnetic field and the magnetic potential is related as

The strain vector, electric field vector and magnetic field vector of the system is expressed in terms of the nodal displacement, nodal electric potential and nodal magnetic potential, respectively as follows

$$\{\varepsilon\} = L_t \{d_t\} = [L_t N_t]\{d_t^e\} = [B_t]\{d_t^e\}$$

$$\{H\} = L_\psi \{\psi\} = [L_\psi N_\psi]\{\psi^e\} = [B_\psi]\{\psi^e\} \quad (7)$$

$$\{E\} = L_\phi \{\phi\} = [L_\phi N_\phi]\{\phi^e\} = [B_\phi]\{\phi^e\}$$

The strain vector, electric field vector and magnetic field vector of the system is expressed in terms of the nodal displacement, nodal electric potential and nodal magnetic potential, respectively as follows

$$\{\varepsilon\} = L_t \{d_t\} = [L_t N_t]\{d_t^e\} = [B_t]\{d_t^e\}$$

$$\{H\} = L_\psi \{\psi\} = [L_\psi N_\psi]\{\psi^e\} = [B_\psi]\{\psi^e\} \quad (7)$$

$$\{E\} = L_\phi \{\phi\} = [L_\phi N_\phi]\{\phi^e\} = [B_\phi]\{\phi^e\}$$

where, L_t, L_ψ and L_ϕ are the differential operators and the sub matrices are generally expressed as

$$[B_{ti}] = \begin{bmatrix} \dfrac{\partial n_i}{\partial x} & 0 & 0 \\ 0 & \dfrac{\partial n_i}{\partial y} & 0 \\ 0 & 0 & \dfrac{\partial n_i}{\partial z} \\ 0 & \dfrac{\partial n_i}{\partial z} & \dfrac{\partial n_i}{\partial y} \\ \dfrac{\partial n_i}{\partial z} & 0 & \dfrac{\partial n_i}{\partial x} \\ \dfrac{\partial n_i}{\partial y} & \dfrac{\partial n_i}{\partial x} & 0 \end{bmatrix} , \quad [B_{\psi i}] = \begin{bmatrix} -\dfrac{\partial n_i}{\partial x} \\ -\dfrac{\partial n_i}{\partial y} \\ -\dfrac{\partial n_i}{\partial z} \end{bmatrix} ,$$

$$[B_{\phi i}] = \begin{bmatrix} -\dfrac{\partial n_i}{\partial x} \\ -\dfrac{\partial n_i}{\partial y} \\ -\dfrac{\partial n_i}{\partial z} \end{bmatrix} \quad (8)$$

where, $i=1, 2, 3,\dots,8$ represents the node number

2.3 Equations of motion

The governing equations of motion of MEE beam in thermal environment are derived by adopting minimization of the total potential energy principle as follows (Kattimani and Ray 2015)

$$T_p = \frac{1}{2}\sum_{k=1}^{N} \left[\begin{cases} \int_{\Omega^k} \delta\{\varepsilon^k\}^T \{\sigma^k\} d\Omega^k - \int_{\Omega^k} \delta[E^k]^T \{D^k\} d\Omega^k \\ -\int_{\Omega^k} \delta[H^k]^T \{B^k\} d\Omega^k - \int_A \delta\{d_t\}^T \{F_{surface}\} dA \\ -\int_{\Omega^k} \delta\{d_t\}^T \{F_{body}\} d\Omega^k - \delta\{d_t\}^T \{F_{conc}\} \\ -\int_A \delta\phi \ Q^\phi dA - \int_A \delta\psi \ Q^\psi dA \end{cases} \right] = 0 \quad (9)$$

where, $k =1, 2, 3, \dots , N$ denotes the layer number. Ω^k and A denotes the volume and area, respectively of the kth layer. $\{F_{surface}\}$, $\{F_{body}\}$ and $\{F_{conc}\}$ are the surface force, the body force and the point load acting on the beam. The electric and magnetic charge densities are represented by Q^ϕ and Q^ψ, respectively. By substituting Eq. (2) in the Eq. (9) we obtain

$$T_p^e = \frac{1}{2}\sum_{k=1}^{N} \left[\begin{cases} \int_{\Omega^k} \{\varepsilon^k\}^T [C_{V_f}^k]\{\varepsilon^k\} d\Omega^k - \int_{\Omega^k} \{\varepsilon^k\}^T [e_{V_f}^k]\{E^k\} d\Omega^k - \int_{\Omega^k} \{\varepsilon^k\}^T [q_{V_f}^k]\{H^k\} d\Omega^k \\ -\int_{\Omega^k} \{\varepsilon^k\}^T [C_{V_f}^k]\{\alpha_{V_f}^k\}\Delta T d\Omega^k - \int_{\Omega^k} \{E^k\}^T [e_{V_f}^k]^T \{\varepsilon^k\} d\Omega^k - \int_{\Omega^k} \{E^k\}^T [\eta_{V_f}^k]\{E^k\} d\Omega^k \\ -\int_{\Omega^k} \{E^k\}^T [m_{V_f}^k]\{H^k\} d\Omega^k - \int_{\Omega^k} \{E^k\}^T [p_{V_f}^k]\Delta T d\Omega^k - \int_{\Omega^k} \{H^k\}^T [q_{V_f}^k]^T \{\varepsilon^k\} d\Omega^k \\ -\int_{\Omega^k} \{H^k\}^T [m_{V_f}^k]\{E^k\} d\Omega^k - \int_{\Omega^k} \{H^k\}^T [\mu_{V_f}^k]\{H^k\} d\Omega^k - \int_{\Omega^k} \{H^k\}^T \{\tau_{V_f}^k\}\Delta T d\Omega^k \\ -\int_A \{d_t\}^T \{F_{surface}\} dA - \int_{\Omega^k} \{d_t\}^T \{F_{body}\} d\Omega^k - \{d_t\}^T \{F_{conc}\} - \int_A \{\phi\} Q^\phi dA - \int_A \{\psi\} Q^\psi dA \end{cases} \right] \quad (10)$$

Further, upon substituting Eq (7) into Eq. (10) we get

$$T_p^e = \frac{1}{2}\sum_{k=1}^{N} \left[\begin{cases} \int_{\Omega^k} \{d_t^e\}^T [B_t]^T [C_{V_f}^k][B_t]\{d_t^e\} d\Omega^k - \int_{\Omega^k} \{d_t^e\}^T [B_t]^T [e_{V_f}^k][B_\phi]\{\phi^e\} d\Omega^k - \int_{\Omega^k} \{d_t^e\}^T [B_t]^T [q_{V_f}^k][B_\psi]\{\psi^e\} d\Omega^k \\ -\int_{\Omega^k} \{d_t^e\}^T [B_t]^T [C_{V_f}^k]\{\alpha_{V_f}^k\}\Delta T d\Omega^k - \int_{\Omega^k} \{\phi^e\}^T [B_\phi]^T [e_{V_f}^k]^T [B_t]\{d_t^e\} d\Omega^k - \int_{\Omega^k} \{\phi^e\}^T [B_\phi]^T [\eta_{V_f}^k][B_\phi]\{\phi^e\} d\Omega^k \\ -\int_{\Omega^k} \{\phi^e\}^T [B_\phi]^T [m_{V_f}^k][B_\psi]\{\psi^e\} d\Omega^k - \int_{\Omega^k} \{\phi^e\}^T [B_\phi]^T [p_{V_f}^k]\Delta T d\Omega^k - \int_{\Omega^k} \{\psi^e\}^T [B_\psi]^T [q_{V_f}^k]^T [B_t]\{d_t^e\} d\Omega^k \\ -\int_{\Omega^k} \{\psi^e\}^T [B_\psi]^T [m_{V_f}^k][B_\phi]\{\phi^e\} d\Omega^k - \int_{\Omega^k} \{\psi^e\}^T [B_\psi]^T [\mu_{V_f}^k][B_\psi]\{\psi^e\} d\Omega^k - \int_{\Omega^k} \{\psi^e\}^T [B_\psi]^T \{\tau_{V_f}^k\}\Delta T d\Omega^k \\ -\int_A \{d_t^e\}^T [N_t]^T \{F_{surface}\} dA - \int_{\Omega^k} \{d_t^e\}^T [N_t]^T \{F_{body}\} d\Omega^k - \{d_t^e\}^T [N_t]^T \{F_{conc}\} - \{\phi^e\}^T F_\phi^e - \{\psi^e\}^T F_\psi^e \end{cases} \right] \quad (11)$$

Simplification of Eq. (11) yields

$$[K_{tt}^e]\{d_t^e\} + [K_{t\phi}^e]\{\phi^e\} + [K_{t\psi}^e]\{\psi^e\} = \{F_m^e\} + \{F_{th}^e\}$$

$$[K_{t\phi}^e]^T \{d_t^e\} - [K_{\phi\phi}^e]\{\phi^e\} - [K_{\phi\psi}^e]\{\psi^e\} = \{F_\phi^e\} - \{F_{p.e}^e\} \quad (12)$$

$$[K_{t\psi}^e]^T \{d_t^e\} - [K_{\phi\psi}^e]^T \{\phi^e\} - [K_{\psi\psi}^e]\{\psi^e\} = \{F_\psi^e\} - \{F_{p.m}^e\}$$

in which, $[K_{tt}^e]$, $[K_{t\phi}^e]$, $[K_{t\psi}^e]$, $[K_{\phi\phi}^e]$, $[K_{\psi\psi}^e]$ and $[K_{\phi\psi}^e]$ are the elemental elastic stiffness matrix, electro-elastic coupling stiffness matrix, magneto-elastic coupling stiffness matrix, electric stiffness matrix, magnetic stiffness matrix and electro-magnetic stiffness matrix, respectively.

$$[K_{tt}^e] = \sum_{k=1}^{N} \left\{ \int_{\Omega^k} [B_t]^T [C_{V_f}^k][B_t] d\Omega^k \right\} ,$$

$$\left[K_{t\phi}^e \right] = \sum_{k=1}^{N} \left\{ \int_{\Omega^k} \left[B_t \right]^T \left[e_{V_f}^k \right] \left[B_\phi \right] d\Omega^k \right\},$$

$$\left[K_{t\psi}^e \right] = \sum_{k=1}^{N} \left\{ \int_{\Omega^k} \left[B_t \right]^T \left[q_{V_f}^k \right] \left[B_\psi \right] d\Omega^k \right\}$$

$$\left[K_{\phi\phi}^e \right] = \sum_{k=1}^{N} \left\{ \int_{\Omega^k} \left[B_\phi \right]^T \left[\eta_{V_f}^k \right] \left[B_\phi \right] d\Omega^k \right\},$$

$$\left[K_{\phi\psi}^e \right] = \sum_{k=1}^{N} \left\{ \int_{\Omega^k} \left[B_\phi \right]^T \left[m_{V_f}^k \right] \left[B_\psi \right] d\Omega^k \right\},$$

$$\left[K_{\psi\psi}^e \right] = \sum_{k=1}^{N} \left\{ \int_{\Omega^k} \left[B_\psi \right]^T \left[\mu_{V_f}^k \right] \left[B_\psi \right] d\Omega^k \right\} \quad (13)$$

Analogously, the various elemental load vectors described in Eq. (12) are the elemental mechanical load vector $\{F_m^e\}$, the elemental thermal load vector $\{F_{th}^e\}$, the elemental electric charge load vector $\{F_\phi^e\}$, the elemental magnetic current load vector $\{F_\psi^e\}$, the elemental pyroelectric load vector $\{F_{p.e}^e\}$, the elemental pyromagnetic load vector $\{F_{p.m}^e\}$. These load vectors are given by

$$\{F_m^e\} = \int_{\Omega^k} [N_t]^T F_{body.e} d\Omega^k + \int_A [N_t]^T F_{surface} dA + [N_t]^T F_{conc.e},$$

$$\{F_\phi^e\} = \int_A [N_\phi]^T Q^\phi dA, \quad \{F_\psi^e\} = \int_A [N_\psi]^T Q^\Psi dA,$$

$$\{F_{th}^e\} = \sum_{k=1}^{N} \left\{ \int_{\Omega^k} [B_t]^T [C_{V_f}^k] \{\alpha_{V_f}^k\} \Delta T \, d\Omega^k \right\},$$

$$\{F_{p.e}\} = \sum_{k=1}^{N} \left\{ \int_{\Omega^k} [B_\phi]^T \{p_{V_f}^k\} \Delta T d\Omega^k \right\},$$

$$\{F_{p.m}\} = \sum_{k=1}^{N} \left\{ \int_{\Omega^k} [B_\psi]^T \{\tau_{V_f}^k\} \Delta T d\Omega^k \right\}$$

$$(14)$$

The Eq. (12) can be condensed by eliminating the electric and magnetic potentials to obtain Eq. (15). Further, thermal displacements are obtained by solving Eq. (15).

$$[K_{eq}] \{u\} = \{F_{eq}\} \quad (15)$$

Later, $\{\phi\}$ and $\{\psi\}$ are computed from Eq. (12) as follows

$$\{\phi\} = [K_3] \{u\} - [K_2]^{-1} \{F_{\phi\_sol}\}$$

$$\{\psi\} = [K_{\psi\psi}]^{-1} [K_{1\_\psi}] \{u\} + [K_{2\_\psi}] \{F_{p.e}\} - \{F_{p.m}\} [K_{3\_\psi}] \quad (16)$$

The component matrices and the equivalent force vector for the Eq. (15) and Eq. (16) are as follows

$$[K_1] = [K_{\phi t}] - [K_{\psi\phi}][K_{\psi\psi}]^{-1}[K_{\psi t}],$$

$$[K_2] = [K_{\phi\phi}] - [K_{\psi\phi}][K_{\psi\psi}]^{-1}[K_{\phi\psi}],$$

$$[K_3] = [K_2]^{-1}[K_1],$$

$$[K_4] = [K_2]^{-1}[K_{\psi\phi}][K_{\psi\psi}],$$

$$[K_5] = [K_{tt}] + [K_{t\psi}][K_{\psi\psi}]^{-1}[K_{\psi t}],$$

$$[K_6] = [K_{t\phi}] - [K_{t\psi}][K_{\psi\psi}]^{-1}[K_{\phi\psi}],$$

$$[K_7] = [K_5] + [K_6][K_3],$$

$$[K_8] = [K_6][K_2]^{-1},$$

$$[K_9] = [K_{t\psi}][K_{\psi\psi}]^{-1} - [K_6][K_4],$$

$$[K_{eq}] = [K_7]$$

$$[K_{1\_\psi}] = [K_{\psi t}] - [K_{\psi\phi}][K_3],$$

$$[K_{2\_\psi}] = [K_{\psi\psi}]^{-1}[K_{\psi\phi}][K_2]^{-1},$$

$$[K_{3\_\psi}] = [K_{\psi\psi}]^{-1}[K_{\psi\phi}][K_2]^{-1}[K_{\psi\phi}]^T[K_{\psi\psi}]^{-1} + [K_{\psi\psi}]^{-1}$$

$$\{F_{eq}\} = [K_9]\{F_{p.m}\} + [K_8]\{F_{p.e}\} + \{F_{th}\},$$

$$\{F_{\phi\_sol}\} = \{F_{p.e}\} - [K_{\psi\phi}]^T[K_{\psi\psi}]^{-1}\{F_{p.m}\}$$

$$(17)$$

3. Results and discussion

In this section, the static response of conventional three layered MEE beam exposed to different in-plane and through-thickness temperature loads is investigated. In this regard, the FE formulation derived in the preceding section is used. The FE model of the cantilever MEE beam is developed using 3D eight noded brick element. Through the numerical examples, the variation of displacements, electric and magnetic potential and stresses are evaluated along the beam length. The study is extended to analyse the influence of various temperature profiles on the variation of static parameters across the MEE beam thickness. Further, parametric studies are performed to examine the effect of stacking sequence.

### 3.1 Validation of the present FE model

The credibility of the proposed FE formulation is justified by solving a numerical case considered by Kondaiah *et al.* (2012) using the present formulation. To account this problem, the multilayered MEE beam is reduced to homogeneous MEE beam (Kondaiah *et al.* (2012)) by assigning all the three layers of MEE beam with the material properties corresponding to V_f =0.5 BaTiO$_3$, as tabulated in Table 1. The beam geometry, thermal loading and the boundary conditions are maintained identical to Kondaiah *et al.* (2012). From Fig. 2, it is found that the convergence of the transverse *z*- direction displacement U_w with the mesh refinement is good. Hence, for the further studies, a FE mesh with 12 elements and 10 elements in the thickness and length direction respectively is considered. The results depicted in Figs. 3(a)-(d) reveal that the proposed FE formulation is in good agreement with Kondaiah *et al.* (2012). Hence the correctness of the FE formulation is verified.
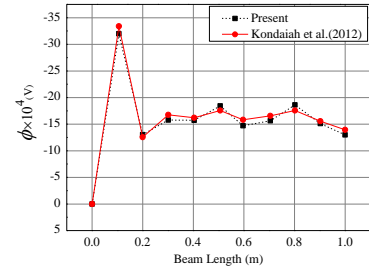
3.2 Effect of stacking sequence

In this section, the effect of stacking sequence i.e., *BFB* MEE beam and *FBF* MEE beam on the direct quantities and the stresses along the beam length and thickness are investigated. The material properties tabulated in Table 1 are used. The magneto-electro-elastic (MEE) beam

Table 1 Material properties corresponding to different volume fraction V_f of BaTiO$_3$–CoFe$_2$O$_4$ (Kondaiah *et al.* 2012)

| Material property	Material constants	0 V_f	0.2 V_f	0.4 V_f	0.5 V_f	0.6 V_f	0.8 V_f	1 V_f
Elastic constants (GPa)	$C_{11}=C_{22}$	286	250	225	220	200	175	166
	C_{12}	173	146	125	120	110	100	77
	$C_{13}=C_{23}$	170	145	125	120	110	100	78
	C_{33}	269.5	240	220	215	190	170	162
	$C_{44}=C_{55}$	45.3	45	45	45	45	50	43
	C_{66}	56.5	52	50	50	45	37.5	44.5
Piezoelectric constants (C/m^2)	e_{31}	0	-2	-3	-3.5	-3.5	-4	-4.4
	e_{33}	0	4	7	9.0	11	14	18.6
	e_{15}	0	0	0	0	0	0	11.6
Dielectric constant (10^{-9} C^2/Nm^2)	$\varepsilon_{11}=\varepsilon_{22}$	0.08	0.33	0.8	0.85	0.9	1	11.2
	ε_{33}	0.093	2.5	5	6.3	7.5	10	12.6
Magnetic permeability (10^{-4} Ns^2/C^2)	$\mu_{11}=\mu_{22}$	-5.9	-3.9	-2.5	-2.0	-1.5	-0.8	0.05
	μ_{33}	1.57	1.33	1	0.9	0.75	0.5	0.1
Piezomagnetic constants (N/Am)	q_{31}	580	410	300	350	200	100	0
	q_{33}	700	550	380	320	260	120	0
	q_{15}	560	340	220	200	180	80	0
Magneto-electric constant (10^{-12}Ns/VC)	$m_{11}=m_{22}$	0	2.8	4.8	5.5	6	6.8	0
	m_{33}	0	2000	2750	2600	2500	1500	0
Pyroelectric constant (10^{-7} C/m^{2}K)	p_2	0	-3.5	-6.5	-7.8	-9	-10.8	0
Pyromagnetic constant (10^{-5} C/m^{2}K)	τ_2	0	-36	-28	-23	-18	-8.5	0
Thermal expansion coefficient (10^{-6} K^{-1})	$\alpha_1=\alpha_2$	10	10.8	11.8	12.3	12.9	14.1	15.7
	α_3	10	9.3	8.6	8.2	7.8	7.2	6.4
Density (kg/m^3)	ρ	5300	5400	5500	5550	5600	5700	5800
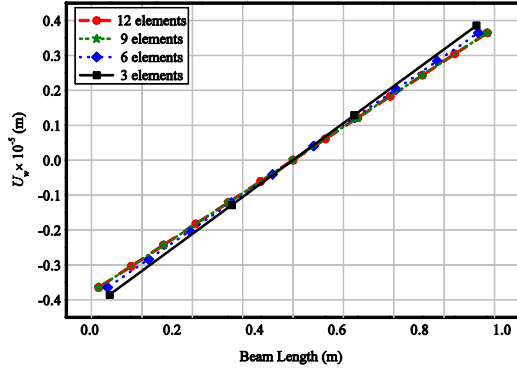
Fig. 2 Convergence of transverse displacement component U_w
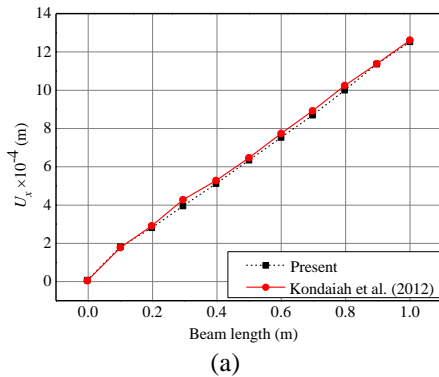
(a)

Fig. 3 Validation of (a) longitudinal *x*-direction U_x (b) electric potential ϕ (c) magnetic potential ψ (d) normal stress-σ_x

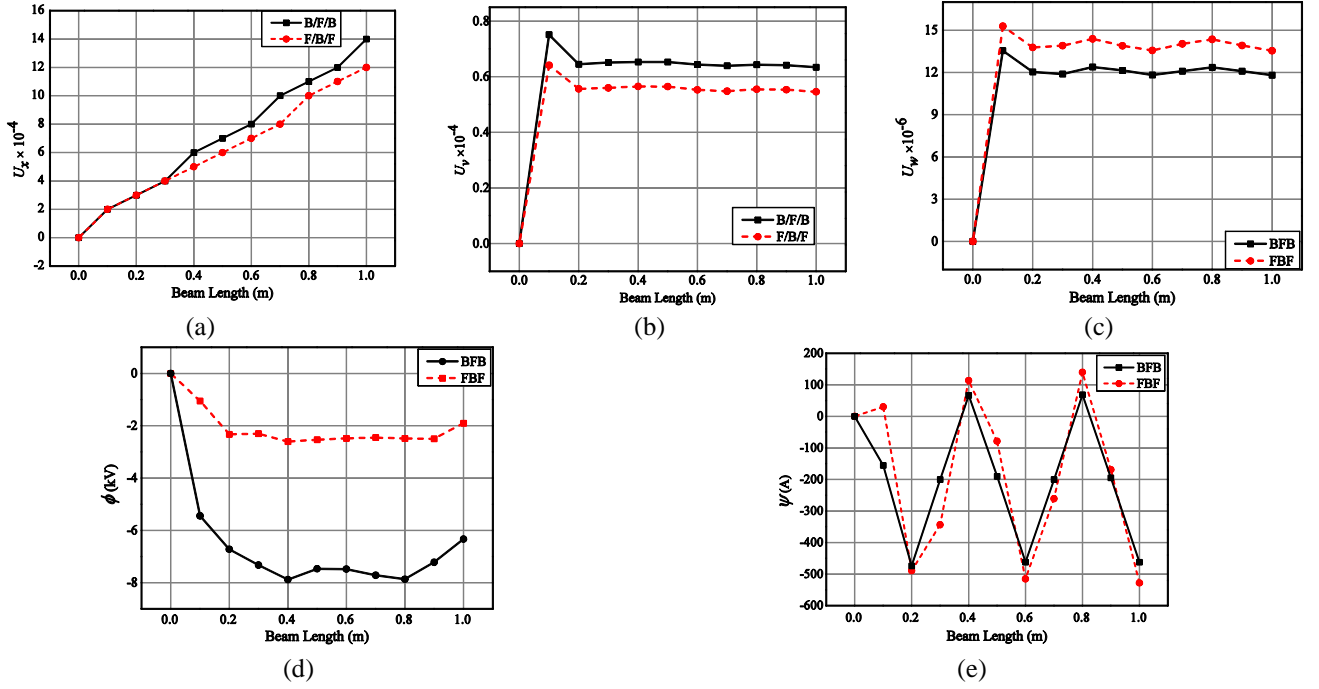
(b)
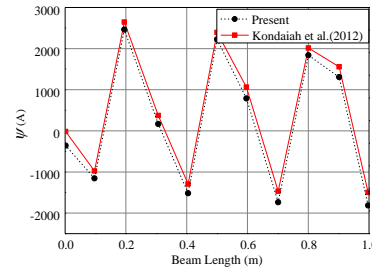
(c)
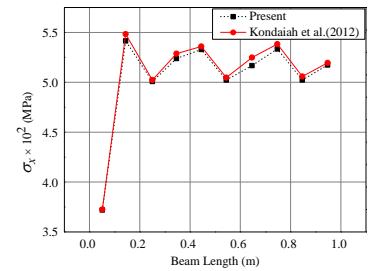
(d)

Fig. 3 Countined

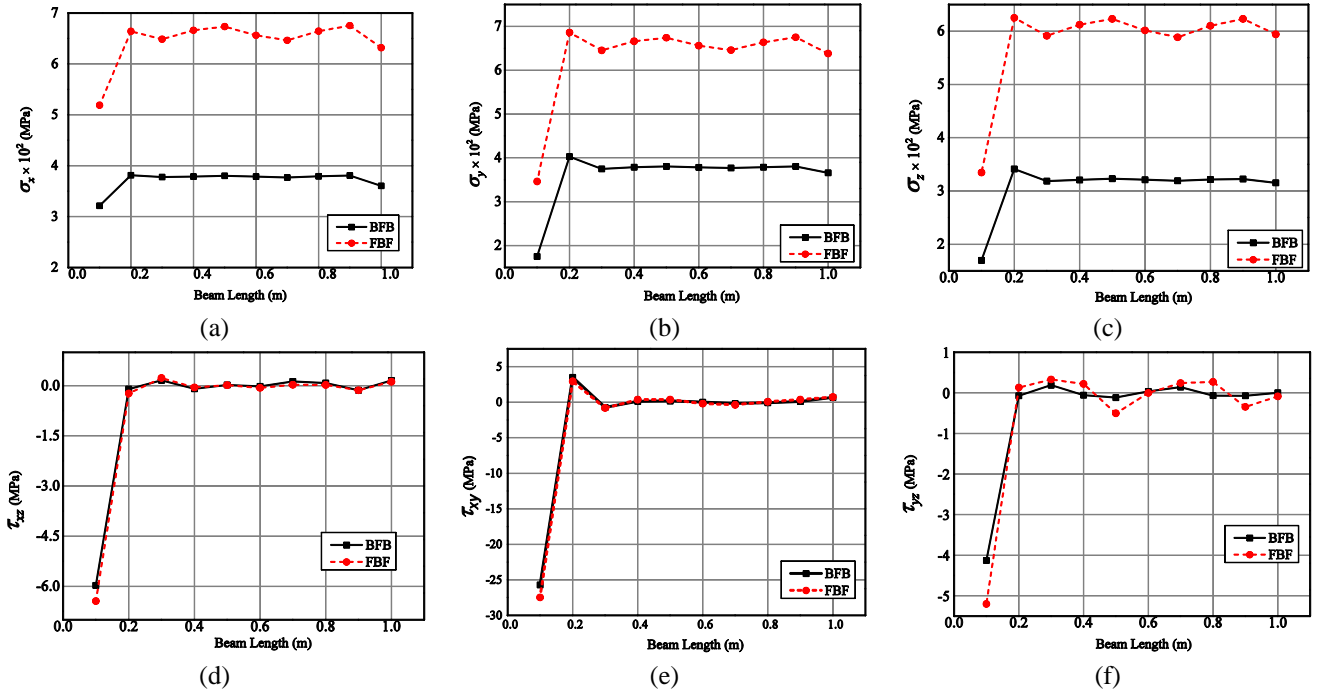Fig. 4 Effect of stacking sequence on displacement components and potentials (a) U_x (b) U_v (c) U_w (d) ϕ (e) ψ

Fig. 5 Effect of stacking sequence on normal stress and shear stress (a) σ_x (b) σ_y (c) σ_z (d) τ_{xz} (e) τ_{xy} (f) τ_{yz}

subjected to a uniform temperature rise of 100 K is considered for the analysis. From Figs. 4(a)-(c) it may be observed that *BFB* stacked MEE beam experiences a higher magnitude of longitudinal *x*-direction displacement component U_x and longitudinal *y*-direction displacement component U_v, whereas the transverse *z*-direction displacement component U_w is higher for *FBF* stacked MEE beam. Likewise, from Figs. 4(d) and (e) it may be observed that the *BFB* and *FBF* MEE beams have a predominant effect on the electric and magnetic potential,

respectively. It may be attributed to the number of layers of $BaTiO_3$ and $CoFe_2O_4$ present in the layup.

Figs. 5(a)-(c) illustrate the variations of the normal stresses σ_x, σ_y and σ_z, respectively. The MEE beam with *FBF* stacking sequence has a higher stress magnitude than *BFB* MEE beam. Further, for both the stacking sequence the maximum values of the stresses are observed near the clamped end. The normal stresses of the *BFB* MEE beam remains almost constant over the beam span, whereas a noticeable discrepancies exists for the *FBF* MEE beam. The
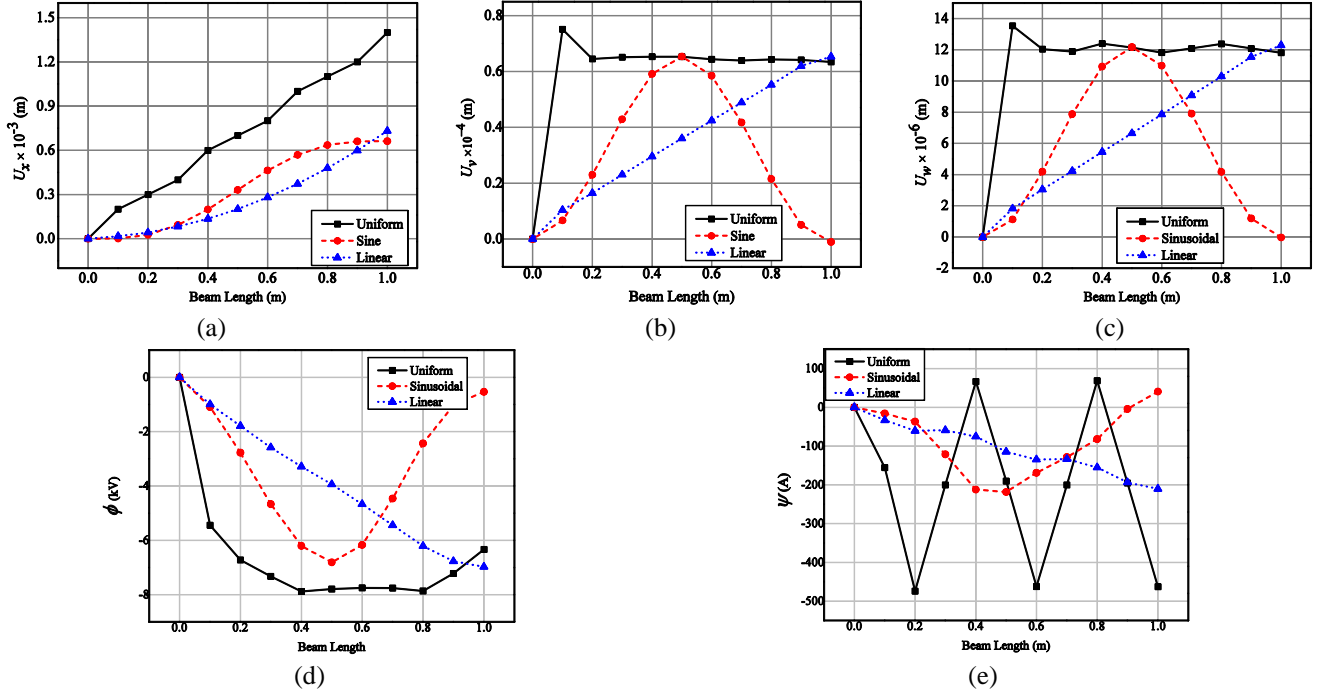
Fig. 6 Effect of different temperature profiles on displacements and potentials (a) U_x (b) U_v (c) U_w (d) ϕ (e) ψ
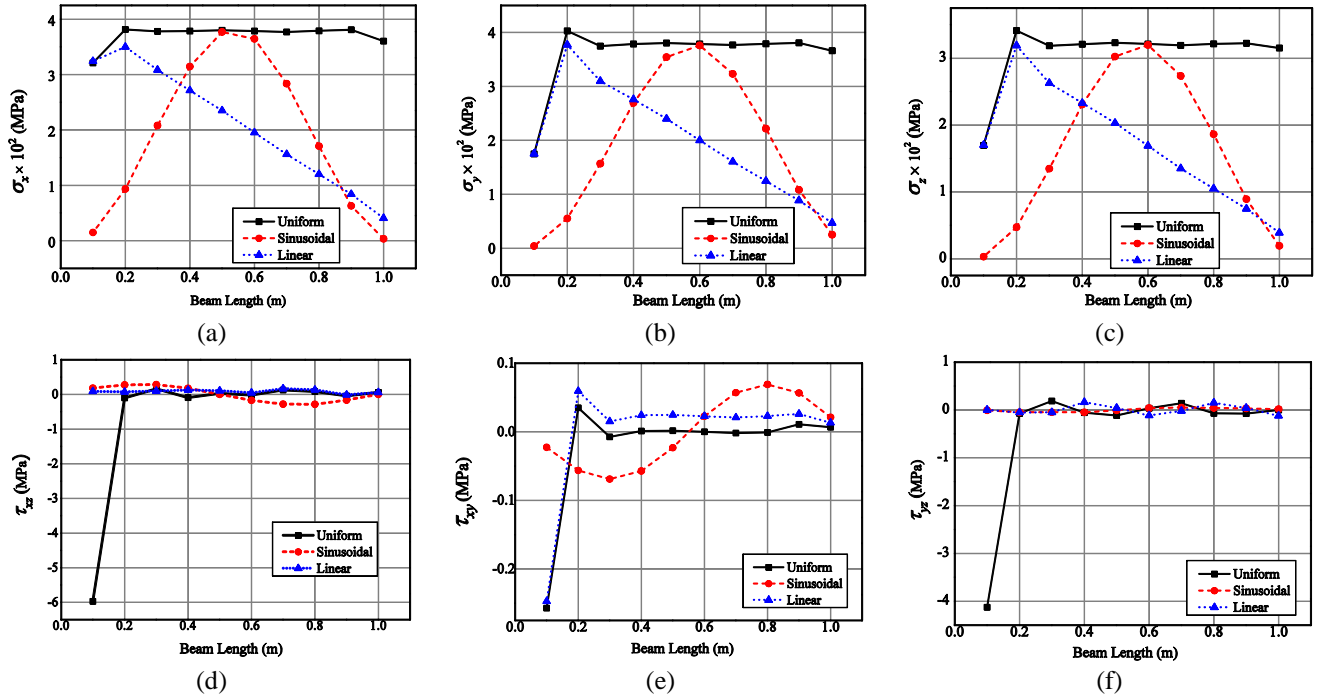

Fig. 7 Effect of different temperature profiles on normal and shear stresses (a) σ_x (b) σ_y (c) σ_z (d) τ_{xz} (e) τ_{xy} (f) τ_{yz}.

shear stresses τ_{xy} and τ_{xz} follow a similar trend of variation for both *BFB* and *FBF* MEE beam as depicted in Figs. 5(d)-(e). From Fig. 5(f) a slightly higher magnitude of τ_{yz} may be noticed that *FBF* MEE beam.

3.3 Effect of various temperature profiles

The various one dimensional temperature profiles varying along the length of the multilayered MEE beam is considered for the analysis. They are as follows:

3.3.1 Uniform temperature profile

The temperature of the MEE beam is uniformly raised from a reference temperature of T_0 to the final temperature of T_{max}. For the ease of calculation T_0 is assumed to be 0 K. The general temperature variation relation can be written as

$$\Delta T = T_{max} - T_0 \tag{18}$$

3.3.2 Half-Sine temperature profile

The MEE beam is analysed for the half-sine temperature

loading. The temperature of the beam is assumed to vary along the length of the beam resembling a half sine wave. The temperature variation can be represented as

$$\Delta T = T_{max}\left\{\sin\left(\frac{\pi x}{L}\right)\right\} \qquad 0 \le x \le L \qquad (19)$$

in which, L is the span length of the beam, x is the point of investigation.

3.3.3 Linearly varying temperature profile

In this case, the temperature varies linearly along the beam length. T_i is the initial temperature at the left end of the beam. The general equation is as follows

$$\Delta T = \{T_{max}\}\, x + \{T_i\} \qquad 0 \le x \le L \qquad (20)$$

The influence of the in-plane temperature profiles on the direct quantities (displacements and potential) and the stresses of the MEE beam are analysed and elucidated in Figs. 6 and 7, respectively. It is observed that the difference in the characteristic behavior of the *BFB* and *FBF* MEE beam remains invariant irrespective of the temperature profiles (as discussed in the previous section). Hence for the sake of brevity only the variations of the direct quantities and stresses related to the *BFB* MEE beam is presented. It may be observed from Table 2 that for all the temperature profiles, the maximum electric and magnetic potential is witnessed for *BFB* and *FBF* stacked MEE beam, respectively. This is obvious due to the number of pure piezoelectric and piezomagnetic phase present in the respective stacking sequence. From Fig. 6(a) it may be noticed that for all the temperature profiles maximum displacement component U_x is observed at the free end of the cantilever MEE beam. Meanwhile, U_v and U_w follow a similar trend of variation as shown in Figs. 6(b) and (c). Maximum values of these displacement components are witnessed at the region near the clamped end for the uniform temperature loading, whereas for sinusoidal and linear temperature profile it is noticed at the midspan and the free end of the MEE beam, respectively. The electric and magnetic potential distribution is represented by Fig. 6(d) and Fig. 6(e), respectively. Among the in-plane temperature profiles considered, the maximum magnitude of these potentials is obtained for the uniform temperature loading. The electric potential varies linearly along the beam length for linear temperature profile. For the MEE beam subjected to sinusoidal temperature loading, the electric potential is maximum at the midspan of the beam. This may be due to the maximum value of the temperature acting at the corresponding region of the beam.

The numerical study is extended to investigate the cross-

Table 2 Effect of various in-plane temperature loads on the maximum electric potential (ϕ_{max}) and maximum magnetic potential ψ_{max} of *BFB* and *FBF* MEE beam

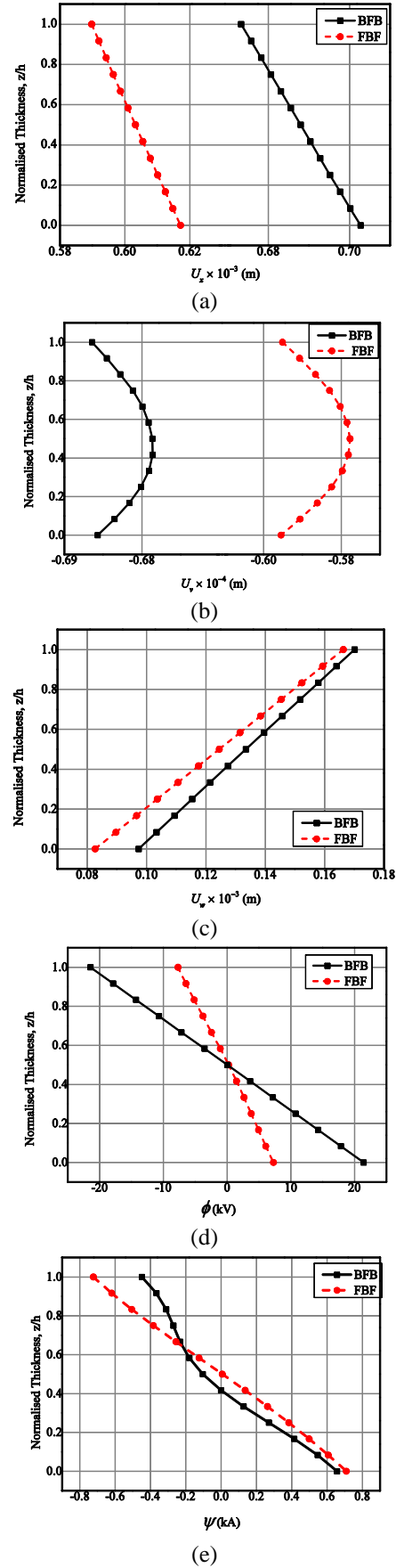| In-plane temperature profile	ϕ_{max} (kV)		ψ_{max} (A)	
	BFB	*FBF*	*BFB*	*FBF*
Uniform	-7.9	-3.1	-474.2	-528.3
Sinusoidal	-6.8	-2.2	-218.2	-236.6
Linear	-7.0	-2.4	-201.6	-220.4

(a)

(b)

(c)

(d)

(e)

Fig. 8 Comparison of displacement components and potentials (a) U_x (b) U_v (c) U_w (d) ϕ (e) ψ of the *BFB* and *FBF* MEE beams subjected to uniform temperature load

Table 3 Effect of various in-plane temperature loads on the maximum values of through-thickness normal and shear stress of *BFB* and *FBF* MEE beam

In-plane temperature profile	Stacking sequence	$\sigma_x \times 10^2$ (MPa)	$\sigma_y \times 10^2$ (MPa)	σ_z (MPa)	τ_{xz} (MPa)	τ_{xy} (MPa)	τ_{yz} (MPa)
Uniform	*BFB*	3.81	3.76	3.23×10^2	-0.35	-0.17	-0.26
	FBF	6.73	6.74	6.23×10^2	0.65	0.35	-0.42
Sinusoidal	*BFB*	3.67	3.5	3.03	-1.04	-2.31	0.26
	FBF	6.6	6.2	5.71	-1.22	-2.57	0.38
Linear	*BFB*	2.35	2.4	2.03×10^2	0.48	2.45	-0.36
	FBF	4.28	4.3	3.97×10^2	0.85	2.86	4.01

(a)

(b)

(c)

(d)
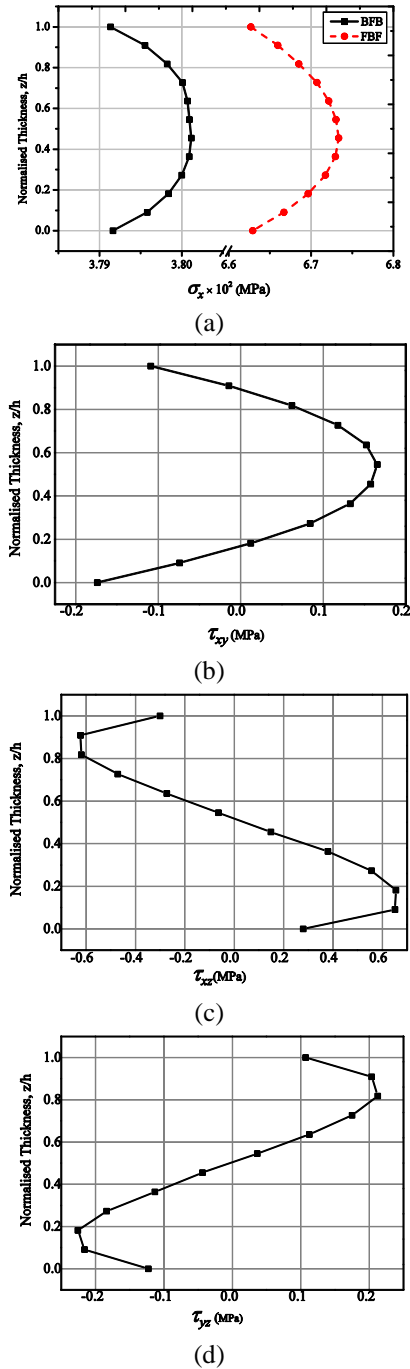
Fig. 9 Through thickness variation of normal and shear stresses (a) σ_x (b) τ_{xy} (c) τ_{xz} (d) τ_{yz} of the MEE beam subjected to uniform temperature load

(a)

(b)

(c)

(d)
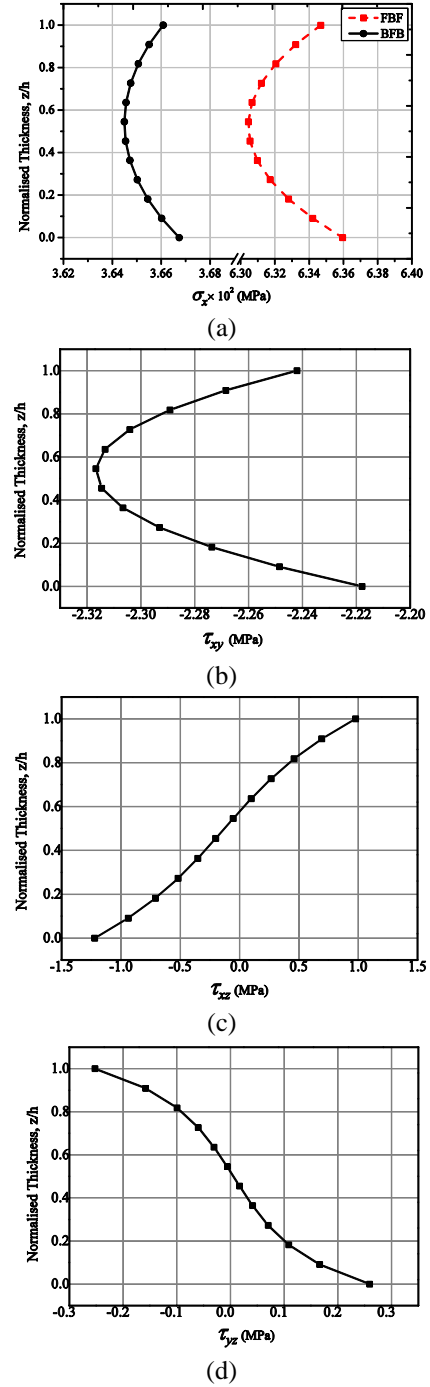
Fig. 10 Through thickness variation of normal and shear stresses (a) σ_x (b) τ_{xy} (c) τ_{xz} (d) τ_{yz} of the MEE beam subjected to sinusoidal temperature load

thickness variations (evaluated at the midspan $x=L/2$) of the direct quantities and the stresses of MEE beam, subjected to in-plane temperature distribution. For the sake of brevity, the variation of the direct quantities (displacements and potentials) corresponding to the multilayered MEE beam subjected to uniform temperature rise of 100 K is alone presented, whereas the stress distribution is plotted for the for all the temperature profile. Figs. 8(a)-(e) illustrate the comparative study of the direct quantities between *BFB* and *FBF* stacking sequence of the MEE beam.
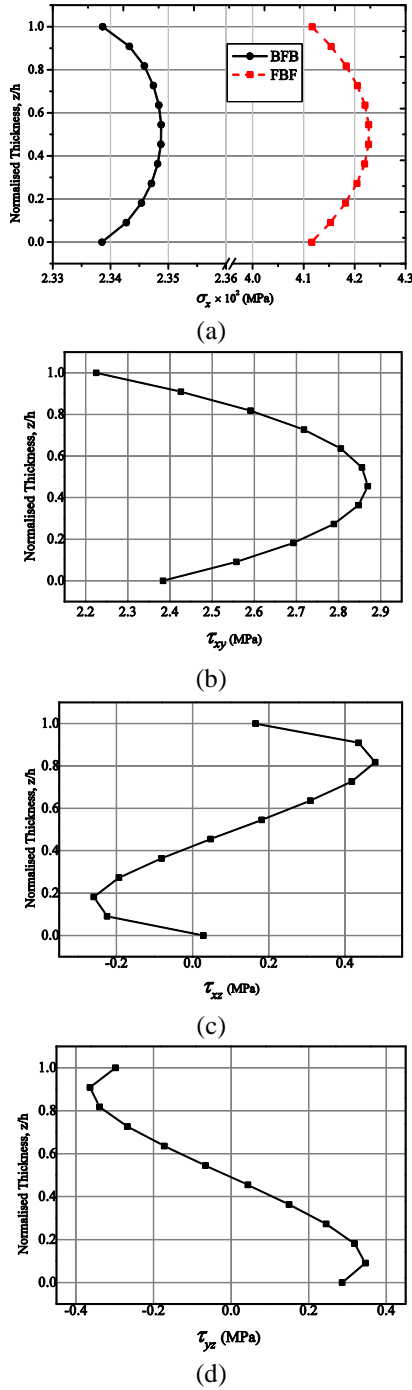
(a)

(b)

(c)

(d)

Fig. 11 Through thickness variation of normal and shear stresses (a) σ_x (b) τ_{xy} (c) τ_{xz} (d) τ_{yz} of the MEE beam subjected to linear temperature load

Further, it is observed that irrespective of the temperature profiles, the normal stresses σ_y and σ_z varies similar to the normal stress σ_x. This holds good for both the stacking sequence considered i.e., *BFB* and *FBF*. Hence the schematic variation of σ_x alone is presented in this study, whereas the comparative study of the maximum values of all the normal and shear stresses is carried out for both the stacking sequence and are tabulated in Table 3. From Fig. 9(a) it may be seen that the stress σ_x has a higher magnitude for *FBF* MEE beam and it is maximum at the middle layer

of the beam for both the stacking sequence. The shear stresses τ_{xz} and τ_{yz} varies symmetrically about the mid layer of the MEE beam as shown in Figs. 9(c) and (d) respectively. The slope drastically changes near the interface of the piezoelectric and piezomagnetic material. Further, it varies almost linearly along the mid section of the beam consisting of pure piezomagnetic material.

Additionally, the influence of the sinusoidal and linear temperature profile on the stresses of the MEE beam is investigated. Figs. 10(a)-(d) show the variation of σ_x, τ_{xy}, τ_{xz} and τ_{yz} respectively of the MEE beam subjected to sinusoidal temperature profile. From Fig. 10(a) it can be observed that the variation of the normal stress σ_x follows a similar trend of variation as that of the MEE beam subjected to uniform temperature load (Fig. 9(a)). Further, a smooth variation in the τ_{xz} and τ_{yz} is noticed along the beam thickness as depicted in Figs. 10(c) and (d).

Likewise, Figs. 11(a)-(d) show the variation of σ_x, τ_{xy}, τ_{xz} and τ_{yz} respectively of the MEE beam subjected to linear temperature profile.

3.5 Temperature profile varying along the beam thickness

In this study, the MEE beam subjected to different through- thickness varying temperature load is analyzed. The various temperature profiles considered are as follows:

3.5.1 Uniform Temperature profile

The temperature throughout the thickness is considered to be uniform. In general, the temperature profile can be represented as

$$\Delta T = T_{max} - T_{ref} \qquad (21)$$

In this study, the T_{max} and the T_{ref} is assumed to be 100 K and 0 K, respectively.

3.5.2 Linear Temperature profile

The MEE beam is exposed to the temperature distribution varying linearly across the beam thickness according to the relation

$$\Delta T = T_i + T_{max}(z/h) \qquad (22)$$

where, T_i is the temperature of the bottom layer, T_{max} is the maximum temperature attainable and z is the distance of the point of interest from the bottom of the beam.

3.5.3 Bi-triangular temperature profile

For MEE beam subjected to bi-triangular profile, the temperature fields vary through the thickness as follows

$$\begin{aligned} \Delta T &= T_{max}(1-z) & 0 \le z \le h/2 \\ \Delta T &= T_{max}(z) & h/2 \le z \le h \end{aligned} \qquad (23)$$

3.5.4 Parabolic temperature profile

The temperature field when MEE beam exposed to parabolic temperature rise can be defined as

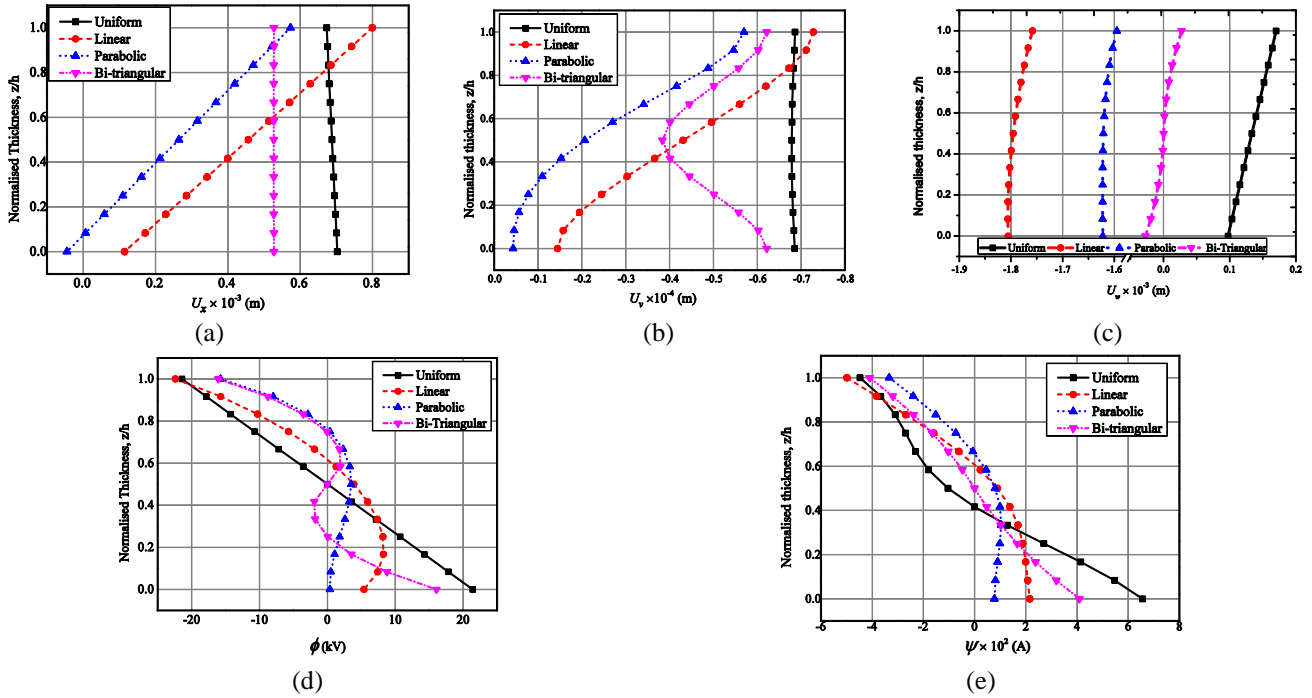$$\Delta T = T_{max}\left\{1 - \left(\frac{z}{h}\right)^2\right\} \qquad 0 \le z \le h \qquad (24)$$

Fig. 16 Effect of various through thickness varying temperature profiles on displacements and potentials (a) U_x (b) U_v (c) U_w (d) ϕ (e) ψ of the *BFB*-MEE beam

Table 4 Effect of various cross-thickness temperature loads on through-thickness variation of the normal and shear stress of *BFB* and *FBF* MEE beam

In-plane temperature profile	Stacking sequence	$\sigma_x \times 10^2$ (MPa)	$\sigma_y \times 10^2$ (MPa)	$\sigma_z \times 10^2$ (MPa)	τ_{xz} (MPa)	τ_{xy} (MPa)	τ_{yz} (MPa)
Uniform	*BFB*	3.7	3.8	3.2	-0.33	-0.16	0.1
	FBF	6.5	6.5	5.9	0.46	-0.4	1.72
Linear	*BFB*	4.4	4.3	3.8	21.8	-0.11	26.1
	FBF	6.5	6.6	6.1	20.0	-0.3	23.5
Parabolic	*BFB*	3.4	3.5	3.1	19.6	-0.06	29.8
	FBF	4.5	4.7	4.2	18.0	-0.2	26.7
Bi-triangular	*BFB*	3.3	3.6	3.1	-0.18	-0.12	22.2
	FBF	5.9	6.1	5.9	0.36	-0.3	19.7

Table 5 Effect of various cross-thickness temperature loads on the maximum electric potential (ϕ) and the maximum magnetic potential (ψ) of various types of MEE beam

Through-thickness temperature profile	ϕ_{max} (kV)		ψ_{max} (A)	
	BFB	*FBF*	*BFB*	*FBF*
Uniform	21.4	-7.7	656.2	723.1
Linear	-22.6	-10.8	-498.6	-582.3
Parabolic	-15.7	-8.3	-333.7	-365.8
Bi-triangular	-16.4	5.6	409.7	532.3

The effect of the temperature profiles mentioned in Eqs. (21)-(24) on the direct quantities and the stresses of the *BFB*-MEE beam are plotted in Figs. 16(a)-(g), respectively. Further, Table 4 correlates the maximum normal and shear stresses developed for *BFB* and *FBF* stacked MEE beam under different cross-thickness temperature profiles. From

Fig. 16(a) negligible variation in the longitudinal *x*-direction displacement component U_x throughout the thickness of the beam may be observed for the uniform and the bi-triangular temperature profile, whereas for the linear temperature profiles it varies according to the temperature distribution. Irrespective of the temperature profile, the maximum value of U_x is observed at the top layer of the MEE beam. From Fig. 16(b) it can be witnessed that the U_v is maximum at the top layer of the MEE beam for the linear and the parabolic temperature profiles whereas, the uniform temperature profile shows almost a constant variation through the thickness. The bi-triangular temperature profile follows a symmetric trend of variation with minimum U_v at the middle layer of the beam, which can be attributed to the temperature distribution. Fig. 16(c) displays the transverse *z*-direction displacement component. The variation of the electric and magnetic potentials of the *BFB* MEE beam is elucidated in Figs. 16(d) and (e) respectively. Further, Figs. 17(a) and (b) displays the variation of electric displacement components D_x and D_z, respectively. Analogously, 17(c) and (d) depicts the magnetic flux density components B_x and B_z, respectively.

The cross thickness stresses σ_x, τ_{xy}, τ_{yz} and τ_{xz} for the various temperature profiles considered are illustrated in Figs. 18(a)-(d), respectively. The maximum normal stress σ_x is observed at the top layer for the parabolic and linear temperature profile, whereas it is minimum at the middle layer for the bi-triangular temperature profile. For all the temperature profiles, the shear stress τ_{xy} varies symmetrically across the middle layer of the beam as elucidated in Fig. 18(b). From Fig. 18(c) it may be observed that the shear stress τ_{yz} is negligible for the uniform temperature profile and its maximum value is observed for the parabolically varying temperature.
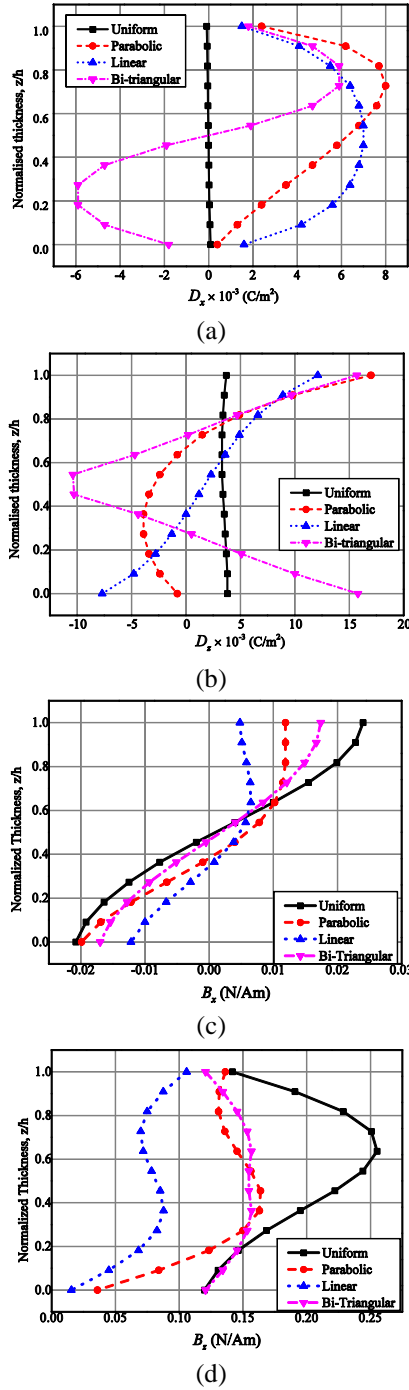
(a)

(b)

(c)

(d)

Fig. 17 Effect of various through thickness varying temperature profiles on (a) electric displacement D_x (b) electric displacement D_z (c) magnetic flux density B_x (d) magnetic flux density B_z of the *BFB*-MEE beam

(a)

(b)

(c)

(d)

Fig. 18 Effect of various through thickness varying temperature profiles on normal and shear stresses (a) σ_x (b) τ_{xy} (c) τ_{yz} (d) τ_{xz} of the *BFB*- MEE beam

4. Conclusions

In the present article, the static behaviour of a conventional multilayered magneto-electro-elastic (MEE) beam exposed to different thermal loads is investigated. In this regard, the governing equations of motion are derived from finite element (FE) method, by employing the minimum total potential energy principle and coupled constitutive equations of MEE material. The condensation
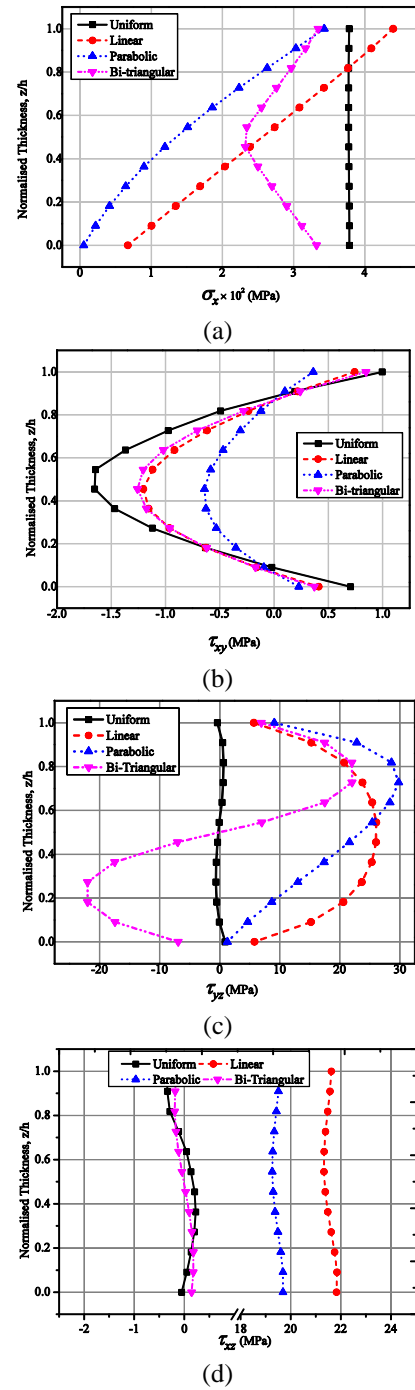
technique is used to solve the global FE equations of motion. Also, in order to show the validity of the proposed FE formulation, the obtained results are compared with the results reported in the literature. Further, a detailed parametric study is carried out to investigate the effects of stacking sequence, in-plane and through thickness temperature profiles on the static parameters of MEE beam. The numerical study reveals that stacking sequence has a significant effect on the displacements and potentials of MEE beam. The x- direction displacement component U_x

and *y*- direction displacement component U_v is observed to be maximum for *BFB* MEE beam. This can be attributed to the reduced stiffness of piezoelectric phase as a result of lesser elastic stiffness co-efficients. The electric potential along the beam length is higher for *BFB* MEE beam. The reason may be due to the presence of more number of pure piezoelectric layers. Analogously, the magnetic potential is more for *FBF* MEE beam. Also, it is notable that the stacking sequence has an insignificant effect on the variation of shear stresses along the beam length. It is evident from the results that among the different temperature profiles considered, the uniform temperature raise is witnessed to have a significant influence on the static behavior of MEE beam. Further, it is also obsreved that the direct quantities are maximum at the region where the highest temperature of the corresponding temperature profile appears. It is believed that the results from the present analysis assist in precise designing of MEE structures in various thermal environments.

References

Akgöz, B. and Civalek, Ö. (2013), "Buckling analysis of linearly tapered micro-columns based on strain gradient elasticity", *Struct. Eng. Mech.,* **48**(2), 195-205.

Akgöz, B. and Civalek, Ö. (2015), "A novel microstructure-dependent shear deformable beam model", *Int. J. Mech. Sci.*, **99**, 10-20.

Akgöz, B. and Civalek, Ö. (2015), "Bending analysis of FG microbeams resting on Winkler elastic foundation via strain gradient elasticity", *Compos. Struct.*, **134**, 294-301.

Alaimo, A., Benedetti, I. and Milazzo, A. (2014), "A finite element formulation for large deflection of multilayered magneto-electro-elastic plates", *Compos. Struct.*, **107**, 643-653.

Ansari, R., Hasrati, E., Gholami, R. and Sadeghi, F. (2015), "Nonlinear analysis of forced vibration of nonlocal third-order shear deformable beam model of magneto-electro-thermo elastic nanobeams", *Compos. Part. B. Eng.*, **83**, 226-241.

Badri, T.M. and Al-Kayiem, H.H, (2013), "Analytical solution for simply supported and multilayered Magneto-Electro-Elastic Plates", *Asian J. Sci. Res.*, **6**, 236-244.

Barati, M.R. and Shahverdi, H. (2016), "A four-variable plate theory for thermal vibration of embedded FG nanoplates under non-uniform temperature distributions with different boundary conditions", *Struct. Eng. Mech.*, **60**(4), 707-727.

Bhangale, R.K. and Ganesan, N. (2006), "Free vibration of simply supported functionally graded and layered magneto-electro-elastic plates by finite element method", *J. Sound Vib.*, **294,** 1016-1038.

Buchanan, G.R. (2004), "Layered versus multiphase magneto-electro-elastic composites", *Compos. Part. B. Eng.*, **35**(5), 413-420.

Chen, J., Chen, H., Pan, E. and Heyliger, P.R. (2007), "Modal analysis of magneto-electro-elastic plates using the state-vector approach", *J. Sound Vib.*, **304**(3-5), 722-734.

Chen, W.Q., Lee, K.Y. and Ding, H.J. (2005), "On free vibration of non-homogeneous transversely isotropic magneto-electro-elastic plates", *J. Sound Vib.*, **279**(1), 237-251.

Civalek, Ö., Demir, C. and Akgöz. B. (2009), "Static analysis of single walled carbon nanotubes (SWCNT) based on Eringen's nonlocal elasticity theory", *Int. J. Eng. Appl. Sci.*, **1**(2), 47-56.

Civalek, Ö., Korkmaz, A. and Demir, C. (2010), "Discrete singular convolution approach for buckling analysis of rectangular Kirchhoff plates subjected to compressive loads on two-

opposite edges", *Adv. Eng. Softw.*, **41**(4), 557-560.

Daga, A., Ganesan, N. and Shankar, K. (2009), "Transient dynamic response of cantilever magneto-electro-elastic beam using finite elements", *Int. J. Comput. Meth. Eng. Sci. Mech.*, **10**(3), 173-185.

Ebrahimi, F. and Barati, M.R. (2016a), "Dynamic modeling of a thermo-piezo-electrically actuated nanosize beam subjected to a magnetic field", *Appl. Phys. A*, **122**, 451.

Ebrahimi, F. and Barati, M.R. (2016b), "Vibration analysis of smart piezoelectrically actuated nanobeams subjected to magneto-electrical field in thermal environment", *J. Vib. Control*, 10.1177/1077546316646239.

Ebrahimi, F. and Jafari, A. (2016), "Thermo-mechanical vibration analysis of temperature-dependent porous FG beams based on Timoshenko beam theory", *Struct. Eng. Mech.*, **59**(2), 343-371.

Hosseini, M. and Dini, A. (2015), "Magneto-thermo-elastic response of a rotating functionally graded cylinder", *Struct. Eng. Mech.*, **56**(1), 137-156.

Huang, D.J., Ding, H.J. and Chen, W.Q. (2010), "Static analysis of anisotropic functionally graded magneto-electro-elastic beams subjected to arbitrary loading", *Eur. J. Mech. A Solid.*, **29**(3), 356-369.

Kaghazian, A., Hajnayeb, A. and Foruzande, H. (2017), "Free vibration analysis of a piezoelectric nanobeam using nonlocal elasticity theory", *Struct. Eng. Mech.*, **61**(5), 617-624.

Kattimani, S.C. and Ray, M.C. (2014), "Active control of large amplitude vibrations of smart magneto-electro-elastic doubly curved shells", *Int. J. Mech. Mater. Des.*, **10**(4), 351-378.

Kattimani, S.C. and Ray, M.C. (2014), "Smart damping of geometrically nonlinear vibrations of magneto-electro-elastic plates", *Compos. Struct.*, **14**, 51-6.

Kattimani, S.C. and Ray, M.C. (2015), "Control of geometrically nonlinear vibrations of functionally graded magneto-electro-elastic plates", *Int. J. Mech. Sci.*, **99,** 154-167.

Ke, L.L. and Wang, Y.S. (2014), "Free vibration of size-dependent magneto-electro-elastic nanobeams based on the nonlocal theory", *Phys. E.*, **63**, 52-61.

Ke, L.L., Wang, Y.S., Yang, J. and Kitipornchai, S. (2014), "Free vibration of size-dependent magnetoelectro-elastic nanoplates based on the nonlocal theory", *Acta. Mech. Sinica.*, **30**(4), 516-525.

Kondaiah, P., Shankar, K. and Ganesan, N. (2012), "Studies on magneto-electro-elastic cantilever beam under thermal environment", *Coupl. Syst. Mech.*, **1**(2), 205-217.

Kondaiah, P., Shankar, K. and Ganesan, N. (2013), "Pyroelectric and pyromagnetic effects on behavior of magneto-electro-elastic plate", *Coupl. Syst. Mech.*, **2**, 1-22.

Kuang, Z.B. (2011), "Physical variational principle and thin plate theory in electro-magneto-elastic analysis", *Int. J. Solid. Struct.*, **48**(2), 317-325.

Kumaravel, A., Ganesan, N. and Sethuraman, R. (2007), "Buckling and vibration analysis of layered and multiphase Magneto-Electro-Elastic beam under thermal environment", *Multidisc. Model. Mater. Struct.*, **3**(4), 461-476.

Kumaravel, A., Ganesan, N. and Sethuraman, R. (2007), "Steady-state analysis of a three-layered electro-magneto-elastic strip in a thermal environment", *Smart Mater. Struct.*, **16**(2), 282-295.

Lage, G.R., Soares, C.M.M., Soares, C.A.M. and Reddy, J.N. (2004), "Layerwise partial mixed finite element analysis of magneto-electro-elastic plates", *Comput. Struct.*, **82**, 1293-1301.

Li, Y.S., Cai, Z.Y. and Shi, S.Y. (2014), "Buckling and free vibration of magnetoelectroelastic nanoplate based on nonlocal theory", *Compos. Struct.*, **111**, 522-529.

Mahieddine, A. and Quali, M. (2008) "Finite element formulation of a beam with piezoelectric patch", *J. Eng. Appl. Sci.*, **3**, 803-807.

Milazzo, A. (2012), "An equivalent single-layer model for

magnetoelectroelastic multilayered plate dynamics", *Compos. Struct.*, **94**(6), 2078-2086.

Milazzo, A. and Orlando, C. (2012), "An equivalent single-layer approach for free vibration analysis of smart laminated thick composite plates", *Smart Mater. Struct.*, **21**(7), 075031.

Milazzo, A., Orlando, C. and Alaimo, A. (2009), "An analytical solution for the magneto-electro-elastic bimorph beam forced vibrations problem", *Smart Mater. Struct.*, **18**(8), 85012.

Moita, J.M.S, Soares, C.M.M. and Soares, C.A.M. (2009), "Analyses of magneto-electro-elastic plates using a higher order finite element model", *Compos. Struct.*, **91**(4), 421-426.

Pan, E. and Heyliger, H. (2002), "Free vibrations of simply supported and multilayered magneto-electro-elastic plates", *J. Sound Vib.*, **252**(3), 429-442.

Pan, E. and Heyliger, P.R. (2003), "Exact solutions for magneto-electro-elastic laminates in cylindrical bending", *Int. J. Solid. Struct.*, **40**(24), 6859-6876.

Phoenix, S.S., Satsangi, S.K. and Singh, B.N. (2009), "Layer-wise modelling of magneto-electro-elastic plates", *J. Sound Vib.*, **324**(3-5), 798-815.

Ramirez, F., Heyliger, P.R. and Pan, E. (2006), "Free vibration response of two-dimensional magneto-electro-elastic laminated plates", *J. Sound Vib.*, **292**, 626-644.

Razavi, S. and Shooshtari, A. (2015), "Nonlinear free vibration of magneto-electro-elastic rectangular plates", *Compos. Struct.*, **119**, 377-384.

Sladek, J., Sladek, V., Krahulec, S. and Pan, E. (2013), "The MLPG analyses of large deflections of magnetoelectroelastic plates", *Eng. Anal. Bound. Elem.*, **37**(4), 673-682.

Sunar, M., Al-Garni, A.Z., Ali, M.H. and Kahraman, R. (2002), "Finite element modeling of thermopiezomagnetic smart structures", *AIAA J.*, **40**, 1845-1851.

Tauchert, T.R. (1996), "Cylindrical bending of hybrid laminates under thermo-electro-mechanical loading", *J. Therm. Stress.*, **19**, 287-296.

Vaezi, M., Shirbani, M.M. and Hajnayeb, A. (2016), "Free vibration analysis of magneto-electro-elastic microbeams subjected to magneto-electric loads", *Phys. E*, **75**, 280-286.

Van Run, A.M.J.G., Terrell, D.R. and Scholing, J.H. (1974), "An in situ grown eutectic magnetoelectric composite material", *J. Mater. Sci.*, **9**(10), 1710-1714.

Wang, J., Chen, L. and Fang, S. (2003), "State vector approach to analysis of multilayered magneto-electro-elastic plates", *Int. J. Solid. Struct.*, **40**(7), 1669-1680.

Wang, X. and Shen, Y. (2002), "The general solution of three-dimensional problems in magnetoelectroelastic media", *Int. J. Eng. Sci.*, **40**(10), 1069-1080.

Xin, L. and Hu, Z. (2015), "Free vibration of layered magneto-electro-elastic beams by SS-DSC Approach", *Compos. Struct.*, **125**, 96-103.

Xue, C.X., Pan, E., Zhang, S.Y. and Chu, H.J. (2011), "Large deflection of a rectangular magnetoelectroelastic thin plate", *Mech. Res. Commun.*, **38**(7), 518-523.

PL